Sodium-Dependent Reorganization of the Sugar-Binding Site of SGLT1[†]

Bruce A. Hirayama,* Donald D. F. Loo, Ana Díez-Sampedro,[‡] Daisy W. Leung,[§] Anne-Kristine Meinild,[∥] Mary Lai-Bing,[⊥] Eric Turk, and Ernest M. Wright

Department of Physiology, The David Geffen School of Medicine at UCLA, 10833 Le Conte Avenue, Los Angeles, California 90095-1751

Received August 3, 2007; Revised Manuscript Received September 18, 2007

ABSTRACT: The sodium-dependent glucose cotransporter SGLT1 undergoes a series of voltage- and ligand-induced conformational changes that underlie the cotransport mechanism. In this study we describe how the binding of external Na changes the conformation of the sugar-binding domain, exposing residues that are involved in sugar recognition to the external environment. We constructed 15 individual Cys mutants in the four transmembrane helices (TMHs) that form the sugar binding and translocation domain. Each mutant was functionally characterized for transport kinetics and substrate specificity. Identification of interactions between mutated residues and hydroxyls on the pyranose ring was assessed by comparing the affinities of deoxy sugars to those of glucose. We determined conformation-dependent accessibility to the mutated residues by both a traditional substituted cysteine accessibility method (SCAM) and a new fluorescence binding assay. These data were integrated to orient the helices and construct a framework of residues that comprise the external sugar binding site. We present evidence that R499, Q457, and T460 play a direct role in sugar recognition and that five other residues are indirectly involved in transport. Arranging the four TMHs to account for Na-dependent accessibility and potential for sugar interaction allows us to propose a testable model for the SGLT1 sugar binding site.

How do cotransporters couple the energy of the transmembrane electrochemical gradient to drive substrates across the membrane? Biochemical, biophysical, and structural studies show that this process involves conformational changes in protein structure. The Na/glucose cotransporter SGLT1[1] is a model for the cotransport process. Chimera and truncation experiments have shown that SGLT1 has a sugar binding and translocation domain in the five C-terminal helices with Na binding located in the N-terminal part of the protein (*1*−*3*). Na binding induces a change in the sugar domain, greatly increasing affinity for sugar, and sugar binding in turn induces another conformation that results in translocation of Na and sugar across the membrane. These processes have been studied in Na^+- and H^+-driven cotransporters via biochemical, electrical, and optical methods to generate kinetic models (*4*−*8*).

We have previously established that Q457, at the external end of transmembrane helix (TMH) XI, interacts with the sugar hydroxyls on carbons 1 and 2 during sugar binding and translocation (*9*) and that this residue is exposed to the external environment only when SGLT1 is in the Na-bound conformation (*10*). In this study we functionally characterized 15 single cysteine mutants in the sugar domain for transport kinetics and substrate specificity. We determined the accessibility of those residues to cysteine-specific reagents by a fluorescence SCAM approach to elucidate how ligands induce structural changes in the sugar binding domain. Integration of these results have identified three residues that are directly involved in sugar binding and translocation, as well as five additional residues with indirect roles.

MATERIALS AND METHODS

Materials. Tetramethylrhodamine-6-maleimide (TMR6M) was purchased from Invitrogen−Molecular Probes (Carlsbad, CA), and sodium (2-sulfonatoethyl) methanethiosulfonate ($MTSES^-$), [2-(trimethylammonium)ethyl] methanethiosulfonate ($MTSET^+$), methyl methanethiosulfonate ($MeMTS^0$), 2-aminoethyl methanethiosulfonate ($MTSEA^+$) and tetramethylrhodamine methanethiosulfonate (TMR-MTS) were from Toronto Research Chemicals (North York, ON, Canada). Deoxy sugars were purchased from Sigma−Aldrich (St. Louis, MO), Toronto Research Chemicals, and CMS (Oxfordshire, U.K.). Capped cRNA was synthesized with kits

[†] This research was supported by Grant DK19567 from the National Institutes of Health.

* Corresponding author. Tel: 310-206-8569. Fax: 310-206-5661. E-mail: bhirayama@mednet.ucla.edu. Lab web page: http://149.142.237.182.

[‡] Present address: Physiology and Biophysics, Miller School of Medicine, University of Miami, Miami, FL 33101.

[§] Present address: Biochemistry, Biophysics and Molecular Biology, Iowa State University, Ames, IA 50011.

[∥] Present address: Institute for Molecular Biology, August Krogh Institute, University of Copenhagen, Copenhagen, Denmark DK-2100.

[⊥] Present address: Emergency Medicine, Weill Medical College of Cornell University/New York-Presbyterian Hospital, New York, NY 10021.

[1] Abbreviations: SGLT1, Na^+/glucose cotransporter SLC5A1; TMH, transmembrane helix; MTS, methanethiosulfonate; TMR6M, tetramethyl rhodamine-6-maleimide; $MTSES^-$, sodium (2-sulfonatoethyl) methanethiosulfonate; $MTSET^+$, [2-(trimethylammonium)ethyl] methanethiosulfonate; $MeMTS^o$, methyl methanethiosulfonate; $MTSEA^+$, 2-aminoethyl methanethiosulfonate; TMR-MTS, tetramethyl rhodamine methanethiosulfonate; Glc, glucose; αMDG, α-methyl-D-glucopyranoside; 1DOG, 1-deoxy-D-glucopyranose; 2DOG, 2-deoxy-D-glucopyranose; 3DOG, 3-deoxy-D-glucopyranose; 4DOG, 4-deoxy-D-glucopyranose; 5Thio, 5-thioglucose; 6DOG, 6-deoxy-D-glucopyranose; TMR, TMR6M or TMR-MTS; a.u., arbitrary units of fluorescence, VCF, voltage clamp fluorometry.

10.1021/bi701562k CCC: $37.00 © 2007 American Chemical Society
Published on Web 10/26/2007

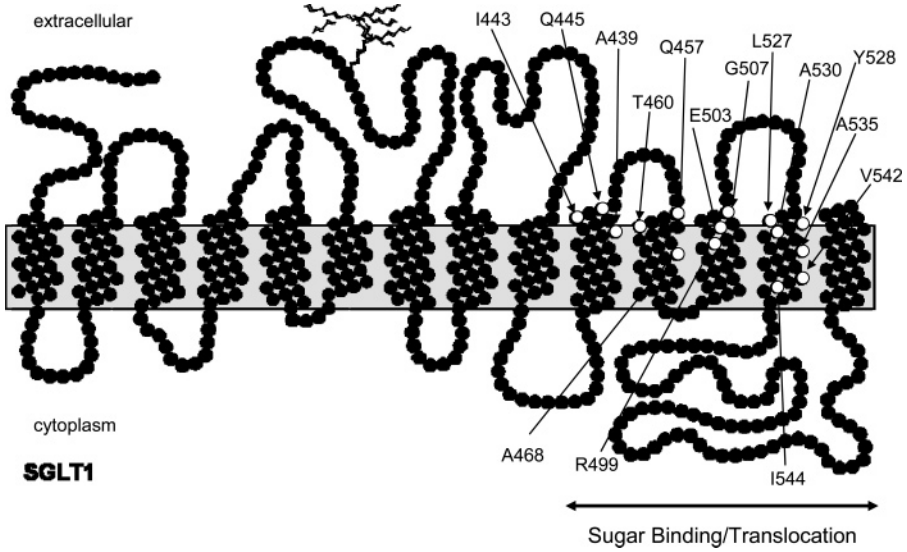

FIGURE 1: Location of engineered Cys residues. Locations of residues mutated to Cys are shown on the topology model of hSGLT1 (*20*). The machinery for sugar transport is contained in the C-terminal five helices of hSGLT1; Na binding and translocation occurs in the N-terminal part of the protein. Helix XIV is missing in some members of the SGLT family, suggesting that it is not necessary for function, therefore we only engineered single Cys mutants in helices X−XIII.

from Ambion (Austin, TX), ^{14}C-D-glucose was purchased from ICN (Costa Mesa, CA), and ^{14}C-α-methyl D-glucopyranoside was from Amersham (GE Healthcare, Piscataway, NJ). *Xenopus laevis* were purchased from either Xenopus 1 (Dexter, MI) or Nasco (Modesto, CA). Enzymes were from New England Biolabs (Ipswich, MA). All other reagents were purchased from Sigma.

hSGLT1 Cys Mutants. Selection of residues for mutagenesis was guided by considering the conserved residues in the SGLT gene family and location of the residue in the topology model. Trafficking of hSGLT1 was shown to be sensitive to mutagenesis, frequently leading to no functional expression because the protein is not inserted into the plasma membrane (*11*). Many other mutations generated were not expressed in oocytes (K. Hager, unpublished observations). Functional mutants were often conservative changes in residues, for example, Ala to Cys or Leu to Cys. Site-directed mutant inserts were generated by standard polymerase chain reaction (PCR) protocols. The PCR products were appropriately digested and ligated into the complimentarily digested hSGLT1 plasmid. Transformation into bacteria, preparation of plasmids, and cRNA synthesis have been previously described (*10*−*12*). The plasmids were sequenced to verify the presence of the mutation and to ensure no errors were introduced in the PCR process. Figure 1 shows the location of the mutants on the secondary structure model. Each hSGLT1 mutant was expressed in *X. laevis* oocytes by injection of cRNA (*10*), and experiments were conducted 3−10 days after injection.

Oocytes. Mature oocytes were isolated from *X. laevis* frogs (see ref *13*). The animal protocols were approved by the University of California Chancellor's Committee on Animal Research and the National Institutes of Health.

Functional Characterization of Mutants. Na-dependent αMDG uptakes were measured in oocytes injected with cRNA of each mutant (*13*). Oocytes were incubated for 15−60 min in the presence of ^{14}C-labeled αMDG (total concentration 50 μM in the presence of Na^+ (Na^+ buffer: 100 mM NaCl, 2 mM KCl, 1 mM $MgCl_2$, 1 mM $CaCl_2$, and 10 mM Tris-Hepes, pH 7.5) or its absence (choline chloride in place of NaCl). Specific SGLT1 uptake was taken as the difference in uptakes in the presence and absence of Na^+ and for each mutant transport was normalized to that obtained for wild-type hSGLT1 in the same batch of oocytes in the same experiment.

Kinetics. The apparent affinities of Na^+ ($K_{0.5}^{Na}$) and sugar ($K_{0.5}^{\alpha MDG}$, $K_{0.5}^{Glc}$) cotransport were measured by use of the two-electrode voltage clamp (*14*). Na^+ kinetics were determined from the 100 mM αMDG-dependent currents as a function of Na^+ concentration, and sugar kinetics were determined from the 100 mM Na^+ currents as a function of sugar concentration. The data were fitted with

$$I = I_{max}([S]^n/(K_{0.5})^n + [S]^n) \quad (1)$$

where I and I_{max} are the current and maximal current, S is substrate, n is the Hill coefficient, and $K_{0.5}$ is the concentration generating $0.5I_{max}$. For sugar kinetics $n = 1$.

Owing to the limited availability and high cost of deoxy sugars and high $K_{0.5}$ values for many mutants, we estimated the mean $K_{0.5}$ for each compound, in at least three different oocytes, using a single concentration close to the $K_{0.5}$ value obtained in a preliminary experiment. Equation 1 was rearranged to eq 2, where I_{max} is that obtained for D-glucose in the same oocyte and I^{test} is the current produced by the test concentration of the deoxy sugar ([test]):

$$K_{0.5}^{test} \sim [test](I_{max} - I^{test})/I^{test} \quad (2)$$

where I_{max} is the value for D-glucose in the same oocyte. The validity of this protocol was confirmed for glucose, αMDG, 1DOG, 2DOG, 5Thio, and 6DOG on wild-type SGLT1, for $K_{0.5}^{sugar}$ ranging from 0.5 mM (glucose) to 112 mM (2DOG), and several mutants. The calculated I_{max} for all sugars was generally 70−110% of $I_{max}^{\alpha MDG}$ determined on the same oocyte (data not shown). Exceptions were noted for individual sugars with some mutants, such as 6DOG for R499C, where the I_{max} was only 25% that for glucose. In

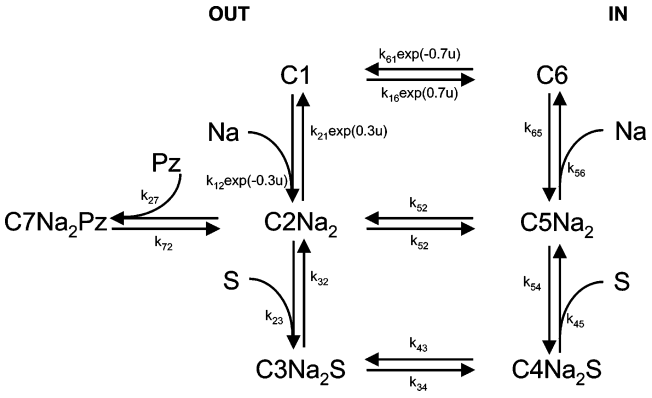

FIGURE 2: Six-state kinetic model for cotransport by hSGLT1. The simplest kinetic model for cotransport by SGLT1 can be described with six states. States C1 and C6 represent the empty transporter in the outside- and inside-facing conformations, C2Na and C5Na are the conformations bound to two Na^+, and C3NaS and C4NaS are also bound to sugar. Two Na^+ ions bind to the transporter before sugar can bind. Binding the competitive inhibitor phlorizin puts SGLT1 into a dead-end state $C7Na_2Pz$. k_{ij} represents the rate constants for transitions between states C*i* and C*j*. Rate constants for transitions between C1, $C2Na_2$, and C6 are voltage-dependent, and $u = FV/RT$, which have their usual thermodynamic meanings. (*6*)

these cases eq 2 was normalized to the estimated I_{max} for the test sugar.

SCAM. The substituted cysteine accessibility method (SCAM, *15*) was used to determine how hSGLT1 conformation affects exposure of specific amino acid positions of a protein (*10*). The method requires creation of Cys mutants and an assay for the binding of cysteine reagents, for example, inhibition of transport. Experiments were done with the oocytes mounted in a continuous-flow chamber on the two-electrode voltage clamp; the bath electrode was equipped with a 3 M KCl agarose bridge to protect the Ag/AgCl electrodes from the reactive cysteine reagents. Measurements of transporter currents were carried out at a membrane holding potential (V_h) of −50 mV with a constant recording of current. After a stable current was observed in Na^+ buffer, we added 5 mM αMDG, which induced an inward current due to the cotransport of two Na^+ ions with each sugar. We then removed the substrates by superfusing the oocyte with choline buffer. This procedure was repeated after each exposure to the cysteine reagent.

The conformation of hSGLT1 was manipulated during the experiment through combinations of substrate, inhibitor, and membrane potential (*6*, *10*). In the presence of Na^+ buffer alone, with $V_h = -100$ mV, the Na-bound outside conformation $C2Na_2$ is favored (occupancy probability $P_o \sim 0.9$); in the absence of Na at $V_h = 0$ mV, the empty inside conformation C6 is most likely ($P_o \sim 0.9$); Na^+ with 100 mM αMDG favors conformation $C5Na_2$ ($P_o \sim 0.6$); and in 500 μM phlorizin, the protein is bound to phlorizin in conformation $C3Na_2Pz$ ($P_o \sim 0.7$) (see Figure 2 and ref *6*).

Location of Cysteine Residue in the Membrane. The membrane potential can exert an electrophoretic effect on charged reagents as well as affecting the distribution of SGLT1 conformations (*10*). The fraction δ of the membrane field sensed by a charged reagent of valence *q* can be estimated from the rate of inhibition (*K*) by a charged ($K^{\pm}$) and an electroneutral (K^0) reagent at two voltages (−50 and −100 mV, eq 3). The latter was estimated from the inhibition of transport by an electroneutral reagent (MeMTS) at two membrane potentials.

$$(K_{-100}{}^0/K_{-50}{}^0)(K_{-100}{}^{\pm}/K_{-50}{}^{\pm}) = \exp(\delta q F \Delta V/RT) \qquad (3)$$

where ΔV is the difference in voltage (50 mV) and *R*, *T*, and *F* have their usual meanings (*16*).

Fluorescent SCAM. Previously we have used transport assays (tracer and electrical) in SCAM studies as the functional assays (*6*, *9*, *10*, *16*). Our SCAM studies of SGLT1 were extended by developing a binding assay based upon the voltage-dependent changes in fluorescence of TMR-labeled Cys mutant protein (ΔF_{max}, see Figure 7) (*6*, *10*, *12*, *18*). No fluorescent response was observed in control experiments with the wild-type protein, indicating that endogenous Cys residues in hSGLT1 and other oocyte proteins are not labeled or that labeled endogenous membrane proteins do not exhibit voltage-dependent fluorescence changes.

The first step was to establish a TMR labeling protocol. The labeling condition for each mutant hSGLT1 protein was determined by varying the concentration of the dye and exposure time in Na^+ buffer to achieve ∼50% of maximal labeling (50% ΔF_{max}). For example, this was achieved for Q457C hSGLT1 by labeling with 100 μM tetramethylrhodamine-6-maleimide (TMR6M) for 10 min, whereas ∼50% labeling of A443C was achieved by labeling with 20 μM TMR6M for 10 min. We then used the predetermined labeling protocol for each mutant and measured ΔF_{max} for oocytes incubated in (i) 100 mM Na^+ buffer, (ii) Na^+ buffer + 100 mM αMDG, (iii) Na^+ buffer + 500 μM phlorizin, or (iv) in the absence of Na^+ (choline replacement). In some experiments tetramethylrhodamine methanethiosulfonate (TMR-MTS) was used for labeling.

Binding of the dye to the engineered Cys was measured after excess dye was washed away in a large volume of Na^+ buffer. The oocytes were mounted in the voltage clamp fluorometry (VCF) chamber (dark pole toward the microscope objective), and the steady-state fluorescence level was subtracted before 100-fold amplification (Warner LPF-8, Hamden, CT, *18*). The membrane was held at −50 mV and the change in fluorescence (expressed in arbitrary units, au) in response to voltage jumps to +50 and −150 mV was then recorded (average of 5−100 sets of pulses).

Reaction rates in Na were estimated from the fluorescence following the method of Pascual and Karlin (*16*) under the conditions of the labeling protocol in Na^+. The second-order rate constant (κ) was estimated as

$$\kappa = (0.5)/([\text{dye}]t) \qquad (4)$$

where [dye] is the concentration of the reactive dye and *t* is the time of exposure in seconds.

Statistical Analysis. Significance of the accessibility data was tested with the analysis of variance macro supplied in Excel (Microsoft, Redmond, WA). Differences between all conditions in the group were considered significant at the 0.01 level. Significant differences between individual conditions were tested by the Tukey HSD method (http://faculty.vassar.edu/lowry/hsd.html), with significance set at the 0.05 level.

Table 1: Summary of Kinetics for hSGLT1 Cys Mutants[a]

helix	mutant	uptake (wt %)	$K_{0.5}^{\alpha MDG}$, mM	$K_{0.5}^{Glc}$, mM	$K_{0.5}^{Na}$, mM
	wt	100	0.7 ± 0.04[b]	0.5 ± 0.02[b]	2.5 ± 0.1[b]
X	A439C	108 ± 6	3.3 ± 0.4	3.0 ± 0.4	2.2 ± 0.3
X	I443C	4 ± 1	0.7 ± 0.1	0.6 ± 0.1	4.3 ± 0.3
X	Q445C	11 ± 1	1.4 ± 0.1	0.8 ± 0.2	1.6 ± 0.6
XI	Q457C	5 ± 1	4.6 ± 0.6[b]	11 ± 1.2[b]	2.5 ± 0.3[c]
XI	T460C	12 ± 3	4.6 ± 0.8	1.6 ± 0.3	6.7 ± 1.2
XI	A468C	12 ± 5	0.5 ± 0.1 0.2 ± 0.1	0.6 ± 0.1	1.3 ± 0.1
XII	R499C	19 ± 1	0.4 ± 0.1 0.7 ± 0.2	0.7 ± 0.1	4.2 ± 2.5
XII	E503C	12 ± 3	0.5 ± 0.1	0.9 ± 0.1 0.6 ± 0.2	3.3 ± 0.1
XII	G507C	73 ± 4	1.0 ± 0.1[d]	0.9 ± 0.6	2.0 ± 0.4[d]
XIII	L527C	16 ± 3	0.4 ± 0.1	0.4 ± 0.1	3.6 ± 1.4
XIII	Y528C	24 ± 4	0.6 ± 0.1	0.4 ± 0.1	3.1 ± 0.8
XIII	A530C	32 ± 3	2.7 ± 1.4	0.8 ± 0.2	2.9 ± 1.5
XIII	A535C	76 ± 8	0.6 ± 0.2 1.0 ± 0.1	0.4 ± 0.1	4.0 ± 1.1
XIII	V542C	83 ± 10	0.6 ± 0.2 0.4 ± 0.1	0.9 ± 0.2	3.4 ± 1.2
XIII	I544C	70 ± 6	0.4 ± 0.1	0.4 ± 0.1 0.7 ± 0.1	2.4 ± 0.5

[a] Apparent transport affinities for sugar ($K_{0.5}^{\alpha MDG}$ and $K_{0.5}^{Glc}$) and Na^+ ($K_{0.5}^{Na}$) are summarized. The relative level of functional expression of mutants was estimated by uptake of αMDG compared to wild type. Functional expression levels ranged from 100% to less than 10% of wild type. All values reported are for a membrane potential of −150 mV and are the mean ± SEM ($n \geq 3$). In those cases with only two experiments, the individual values are reported with error of the estimate for the fit. Previously reported values. [b] References *9* and *22*. [c] Reference *10*. [d] Reference *6*.

Sequence Alignments. The amino acid sequences of 34 members of the SGLT (SLC5) gene family were aligned by use of PIMA 1.4 (http://searchlauncher.bcm.tmc.edu/multi-align/multi-align.html) and maximum linkage clustering. The alignments were checked on a limited number of sequences by use of the CLUSTAL W 1.74 multiple sequence alignment tool (*19*). The sequences included SGLT1 (human, rat, mouse, rabbit, sheep, pig, horse, chicken, and bovine), SGLT2 (human, rat, and mouse), SGLT3 (human, pig, and mouse), SGLT4 (human and mouse), SGLT5 (rabbit and human), SGLT6/SMIT2 (human, rabbit, mouse, and frog), SMIT1 (human, mouse, bovine, and canine), NIS (human, rat, pig, and mouse), and SMV (human, rat, and rabbit). All, apart from NIS, are putative 14 TMH proteins: NIS is missing TMH XIV (*20*, *21*).

RESULTS

Our goal was to determine the rearrangements of helices X−XIII, the sugar binding and translocation domain of hSGLT1, during the cotransport cycle. The approach we used was to produce a series of cysteine mutants and determine (1) the functional consequences of the mutations, (2) the effect of alkylation with MTS reagents, and (3) the accessibility of these cysteines to tetramethylrhodamine-conjugated Cys-reactive reagents (TMR) as a function of conformational state.

Functional Consequences of Mutations. None of the residues replaced with Cys was essential for cotransport. All were shown to be capable of Na^+-dependent αMDG uptake (Table 1) and generated sugar-dependent Na^+ currents. A major effect was on the expression level as measured by radioactive αMDG uptake 3−4 days after cRNA injection. About half the mutants expressed activity at wild-type levels, but the expression level of several was reduced by an order of magnitude. This depended on the residue mutated and most likely was the result of a trafficking defect (*11*). Low expression levels were partially compensated by culturing the oocytes for up to 10 days for the electrical and fluorescence experiments.

The apparent affinities for sugar ($K_{0.5}^{Glc}$, $K_{0.5}^{\alpha MDG}$) and Na^+ transport ($K_{0.5}^{Na}$) were estimated by use of the two-electrode voltage clamp and sugar-dependent Na^+ currents (see Figure 3A,D). Examples of glucose and Na^+ kinetics are shown for Y528C and T460C on four different oocytes (Figure 4). Note that for both mutants the $K_{0.5}^{Na}$ values were similar (4 ± 1 mM and 3 ± 1 mM) compared to the wild-type (2.5 mM). The $K_{0.5}^{Glc}$ for Y528C (0.5 ± 0.05 mM) was unchanged from that of wild type, but in T460C it was increased by a factor of 3 (1.4 ± 0.3 mM). Cotransport is voltage-dependent and increases with hyperpolarization (*14*), so due to the low level of expression of some of the mutants, we report the summary of kinetics at hyperpolarizing potentials (−150 mV, Table 1). For these Cys mutants the changes in $K_{0.5}^{Na}$ compared to the wild type (∼2.5 mM, *10*, *22*) were generally small, with significant changes (∼3-fold) measured only in T460C. In comparison, $K_{0.5}^{Glc}$ increased up to 20-fold for several mutants (A439C, Q457C, and T460C) over the wild-type value (∼0.5 mM; *9*, *10*, *23*), and differences in $K_{0.5}^{Glc}$ and $K_{0.5}^{\alpha MDG}$ were noted for T460C and A530C.

Effect of Conformation on Residue Accessibility. The starting point for this study of the structure of the sugar-binding domain was residue Q457, which is part of the sugar-binding pocket (*9*). Alkylation of the Cys mutant Q457C inactivates the transport mechanism, and SCAM showed that this residue is exposed in the Na^+-bound conformation and is otherwise inaccessible to the external medium (*10*). We applied this method to residue A468, predicted to be on the same side of helix XI as Q457 but further into the membrane

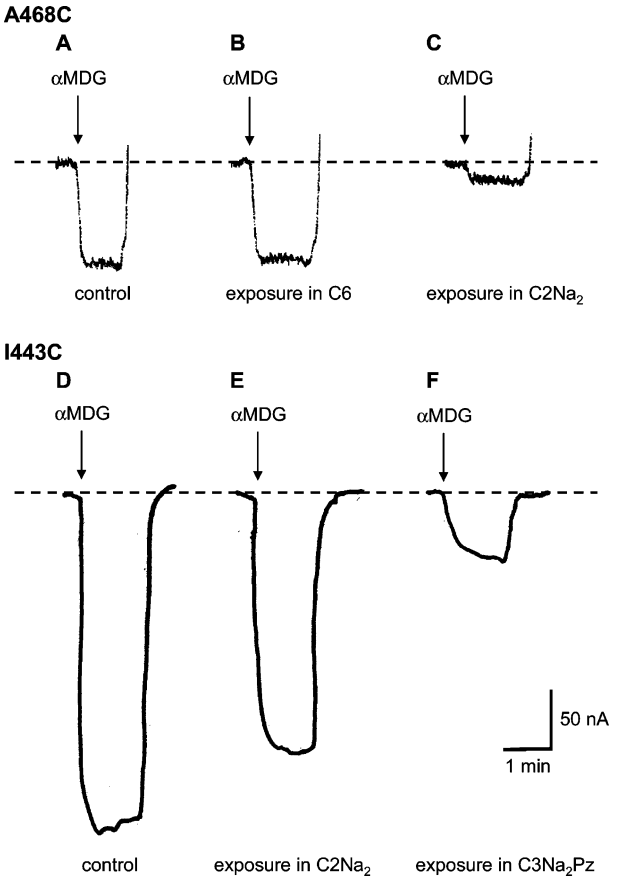

FIGURE 3: Accessibility of A468C and I443C to Cys reagents is dependent on hSGLT1 conformation. Examples of SGLT1 conformational dependence of inactivation of Na^+−sugar cotransport by Cys-specific reagents are shown for oocytes expressing either A468C or I443C hSGLT1. The two-microelectrode voltage clamp was used to continuously monitor the current. In each panel the oocyte was equilibrated in Na^+ buffer to establish a baseline current level (dashed line), and at the arrow αMDG was added to the bath, generating an inward current of Na^+ stoichiometrically coupled to sugar influx (2 Na^+:1 sugar). Superfusing substrate-free buffer at the end of the trial eliminated the current. The top panel shows MeMTS accessibility of A468C was greatest in the Na-bound conformation. (A) Control 5 mM αMDG-induced current. (B) Current generated after exposure to 1 mM MeMTS in the absence of Na^+ at $V_m = 0$ mV, a condition highly favoring conformation C6 (Figure 2), was reduced by 10%. (C) After exposure to 1 mM MeMTS in Na^+ and at $V_m = -100$ mV (a condition highly favoring conformation $C2Na_2$), 90% of the αMDG-induced current was inhibited. The lower panel shows accessibility of I443C to TMR6M was highest in the phlorizin-bound conformation. (D) Control 10 mM αMDG-induced current, 300 nA. (E) After exposure to 20 μM TMR6M in Na^+ buffer for 10 min, the current was reduced by 20%. (F) Exposure to TMR6M in the presence of Na^+ and 500 μM phlorizin reduced the αMDG-induced current by 75%. In all I443C exposures, V_m was −50 mV.

(Figure 1). Figure 3 shows a SCAM experiment on the Cys mutant A468C. Figure 3A shows the starting transport activity. When 5 mM α-methyl D-glucopyranoside (αMDG, arrow) was added to the bathing medium at a holding potential of −50 mV, an inward current of −90 nA was induced, demonstrating Na^+/sugar cotransport (*24*). Removal of the substrates from the bath, eliminating cotransport, reversed the current. The oocyte was then equilibrated in a sodium-free bath (choline buffer), the membrane potential was clamped at 0 mV, and then the sample was exposed to 1 mM methyl methanethiosulfonate (MeMTS) for 5 min.

Table 2: Reactivity of Cys Reagents with hSGLT1 Mutants[a]

		estimated rate constant, M^{-1} s^{-1}		
helix	position	MTSEA	MeMTS	TMR
X	439	<0.1	<0.1	ND, poor signal
X	443	215	5	40
X	445	ND	ND	8
XI	457	23 100	14.6	8
XI	460	39 000	4	8
	468	1[b]	4[b]	not accessible
XII	499	ND	6[b]	not accessible
	503	ND	ND	150
XII	507	ND	ND	83
XIII	527	ND	ND	8
XIII	528	ND		∼1

[a] SGLT1 mutants were expressed in oocytes, and rates of labeling were estimated for MTSEA and MeMTS and for the fluorescent dyes TMR6M and TMR-MTS. For MTSEA and MeMTS, exposure was in Na^+ buffer at $V_m = -50$ mV, unless noted, and rates were estimated from the decrease in sugar-induced current. Mutants in which the current was not reduced by at least 80% in the maximal condition of exposure (up to 10 min at concentrations of 1−5 mM) were not determined (ND). Labeling with the dyes was in Na^+ buffer, in the dark, for a predetermined time and [dye] estimated to inhibit ∼50% of ΔF_{max}. Exposure time was 10 min, except for Y528C, in which the exposure was for 30 min. Rates were estimated with the assumption that the conditions achieved 50% of maximal labeling. Similarly, rate constants for accessibility by the fluorescent dyes could not be determined if the dye concentration/exposure time (500 μM/60 min) did not saturate. [b] Determined at −100 mV.

After washout of the reagent and re-equilibration in Na^+ buffer at $V_h = -50$ mV, addition of 5 mM αMDG induced a current of −80 nA (Figure 3B), indicating that ∼10% of the transporters were inactivated by alkylation with MeMTS. The same oocyte was then exposed to MeMTS, but in Na^+ buffer, with $V_h = -100$ mV. The resulting αMDG current was only −10 nA (Figure 3C), showing that 90% of the transporters were inactivated. This indicates that the Na^+-bound conformation ($C2Na_2$, Figure 2), the predominant conformation in the presence of Na^+ at −100 mV, exposed 468C to the MTS reagents in the external environment. In contrast, the empty facing the cytoplasm conformation (C6, Figure 2), the predominant conformation in the absence of Na^+ at depolarizing potentials, was inaccessible to the MTS reagent, that is, it was shielded from the external medium.

Similar experiments (not shown) indicated that in the $C2Na_2$ conformation both A468C and R499C were exposed to the external medium, and in all other conformations they were shielded. Comparison of the labeling rates between Q457C, A468C, and R499C shows that, even under the most favorable condition ($C2Na_2$), access to residues 468C and 499C is restricted compared to 457C (Table 2), consistent with the position of these two residues being deeper in the membrane than 457C.

A different pattern of accessibility was observed for oocytes expressing I443C hSGLT1. The presence of 10 mM αMDG induced a −300 nA current in the untreated oocyte (Figure 3D), and after re-equilibration in Na^+ buffer, the oocyte was exposed to 20 μM TMR6M for 10 min. This reduced the αMDG-induced current by 20% (Figure 3E). Re-exposure to 20 μM TMR6M for another 10 min, but this time in the presence of 500 μM phlorizin, resulted in inactivation of 75% of the remaining current (Figure 3F), indicating that, in contrast to A468C, I443C is exposed to

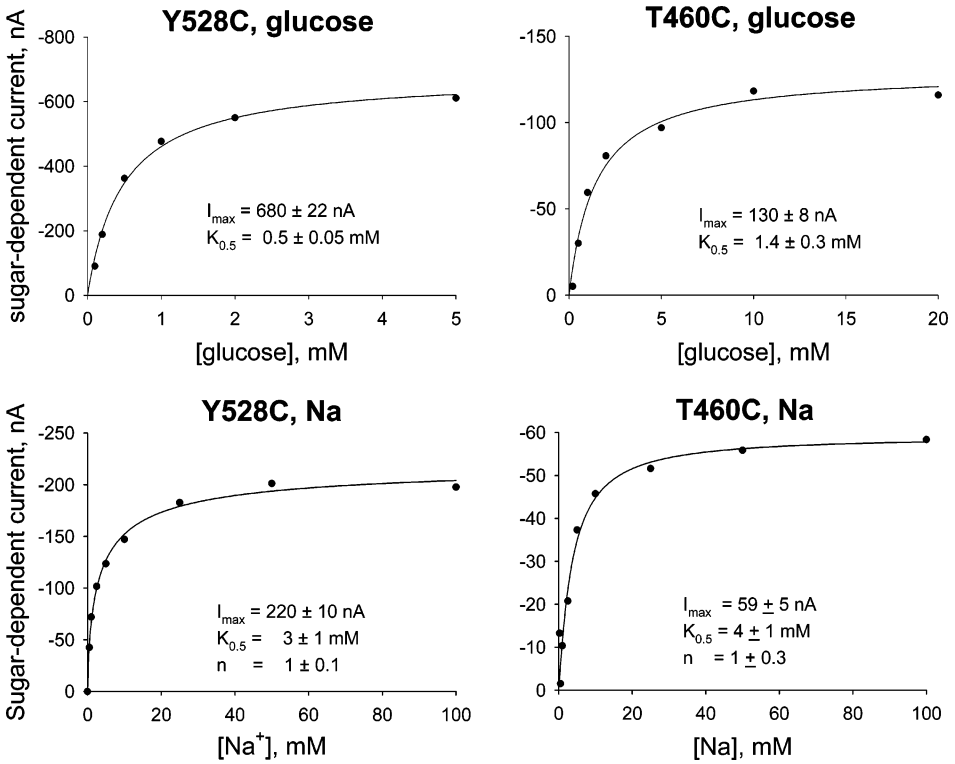

FIGURE 4: Kinetics of Cys mutants: Representative examples. The apparent kinetics of cotransport was determined for sugar and Na^+ for each of the Cys mutants by measurement of sugar-induced currents with the voltage clamp (V_m = −150 mV). Examples of Na^+ and glucose activation data shown here are for Y528C and T460C. Apparent Na^+ affinity ($K_{0.5}^{Na}$ for 100 mM αMDG) was unchanged from the wt values (∼2.5 mM), but for sugar $K_{0.5}^{Glc}$ (for 100 mM Na^+) was higher for T460C and unchanged for Y528C compared to the wt value of ∼0.5 mM. Each figure presents results from an individual oocyte fitted with eq 1. The parameter value is ± error of the fit. Table 1 presents a summary of kinetics for glucose, αMDG, and Na.

the external environment when phlorizin is bound to the protein ($C3Na_2Pz$). Additional experiments showed that binding Na^+ and sugar, state $C5Na_2$ (*6*), gave similar results. We also note that MeMTS inactivated I443C hSGLT1 in a substrate-dependent fashion, but the effect was less dramatic (not shown). This suggests small molecules like MeMTS have access to I443C in states other than $C3Na_2Pz$, where the larger dyes are sterically excluded.

The MTS reagents, negatively charged sodium (2-sulfonatoethyl) methanethiosulfonate ($MTSES^-$) and positively charged [2-(trimethylammonium)ethyl] methanethiosulfonate ($MTSET^+$), were also able to inactivate A468C. We took advantage of this observation and our ability to manipulate the membrane potential to estimate the position of A468C in the membrane electric field (*16*). A468C oocytes were exposed to $MTSES^-$, $MeMTS^0$, or $MTSET^+$ in Na^+ buffer at either V_h −50 or −100 mV, and the rate of inactivation of the αMDG current for each combination was determined (Figure 5). The rate of inactivation by $MTSET^+$ was enhanced 4-fold at −100 mV compared to −50 mV; conversely, hyperpolarization appeared to reduce (not significantly) inactivation by the negatively charged $MTSES^-$. Taking into account the effect of V_h on SGLT1 conformation in Na^+ from the difference in $MeMTS^0$ inactivation (increased accessibility at hyperpolarizing potentials, $K_{-100}^0/K_{-50}^0 = 1.5$), estimating the electrophoretic effect for the charged reagents ($K_{-100}^{\pm}/K_{-50}^{\pm}$) to be 2.5 for MTSET and 0.5 for MTSES, and applying eq 2 indicated that 468 is located halfway through the membrane field (49% ± 11%, $n = 3$).

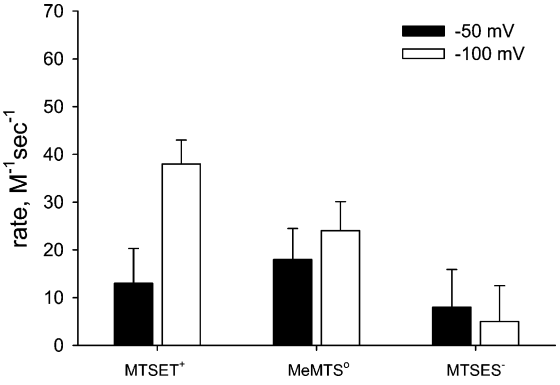

FIGURE 5: Effect of membrane potential on labeling of A468C by charged MTS reagents. Reaction rates of the A468C hSGLT1 mutant to neutral ($MeMTS^0$), cationic ($MTSET^+$), and anionic ($MTSES^-$) reagents were determined as a function of membrane potential. The difference in reaction rate of $MeMTS^0$ reflects the influence of membrane potential on SGLT1 conformation. Experiments were done as in Figure 4 with the different MTS reagents in Na^+ buffer and exposure at either V_m = −50 mV or −100 mV. Data is the mean and SEM of at least three different oocytes.

Reagents larger that MeMTS were not able to inhibit R499C. No significiant effects of 1 mM MTSEA on cotransport were detected for A439C, Q445C, E503C, G507C, L527C, Y528C, A539C, A535C, V542C, or I544C. Surprisingly, 0.1 mM TMR-MTS and ThioGlo3 inhibited Q445C cotransport by 70−100% (not shown).

Fluorescence as a Measure of Accessibility. For many of the mutants, transport was not significantly inhibited by Cys reagents, for example, G507C (*6*), and so the traditional SCAM technique is not applicable. We found, however, that

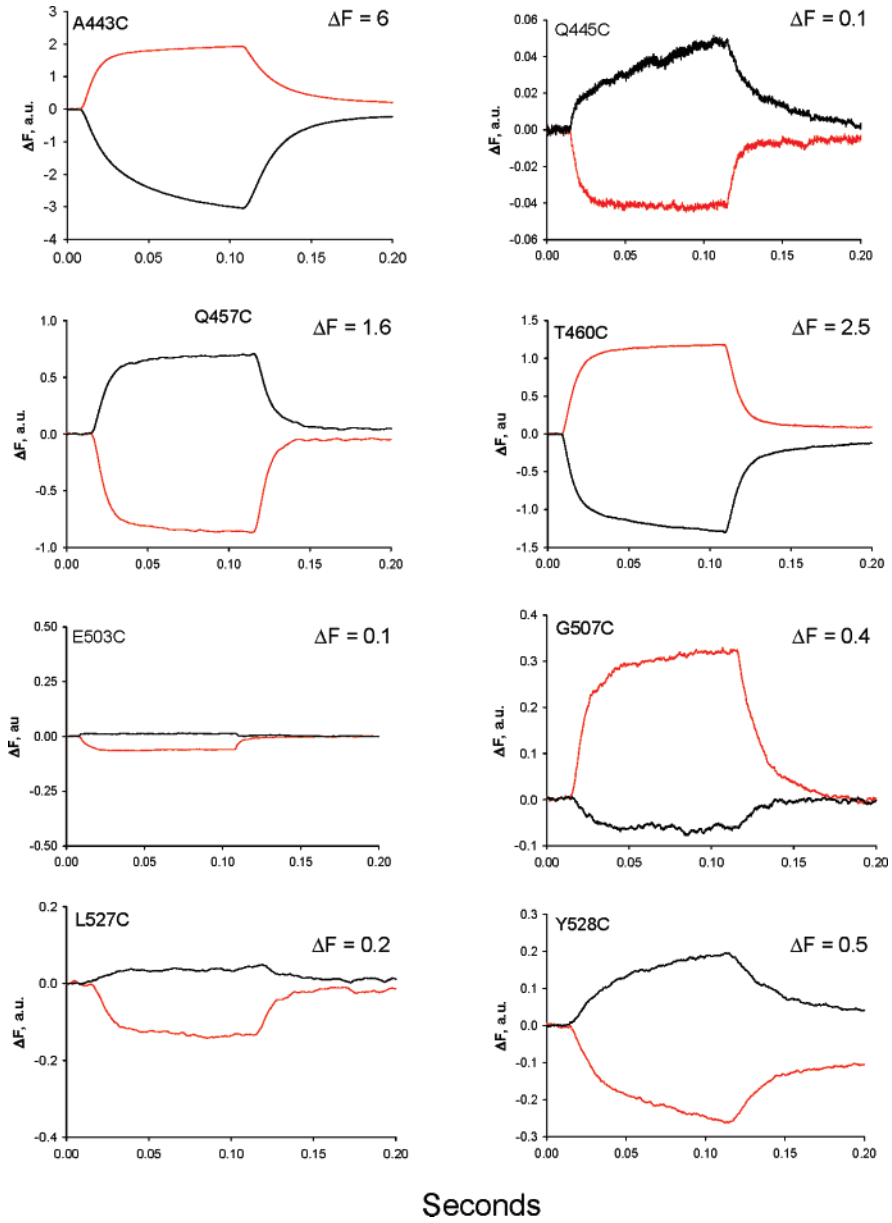

FIGURE 6: Fluorescence traces for Cys mutants labeled with tetramethylrhodamine. Representative fluorescence traces of the eight Cys mutants analyzed in Figure 8 are shown. Oocytes expressing each mutant were labeled with TMR6M as described under Materials and Methods. The membrane potential was held at $V_h = -50$ mV, and responses to depolarizing (red) and hyperpolarizing (black) voltage jumps of ±100 mV from V_h were recorded while the oocytes were bathed in Na^+ buffer. Note the differences in scaling of ΔF.

most of the mutants in this study could be labeled with fluorescent dyes. Even if there was no change in function, all dye-conjugated mutants exhibited changes in fluorescence in response to jumps in membrane potential, ΔF (Figure 6). Each panel depicts the fluorescence response of a TMR-labeled mutant to a ±100 mV voltage jump from $V_h = -50$ mV for 100 ms. Measuring the difference in fluorescence between jumps to depolarizing and hyperpolarizing membrane potentials (ΔF) allowed us to measure specific binding of the dye to the target residue on SGLT1. Note that the polarity of the fluorescence varied between the different mutations. For Q457C labeled with TMR6M, depolarizing the membrane resulted in a quench of fluorescence, and hyperpolarizing increased fluorescence. In contrast, in I443 the effect of membrane potential was reversed. The time constant for the fluorescence change also varied by mutated residue: the fluorescence of Q457C-TMR6M was symmetrical (time constant for the medium component of the ON fluorescence $\tau^{med} \sim 10$ ms, *18*), but for I443C-TMR6M, τ^{med} for the depolarizing ON fluorescence (~8 ms) was faster than the hyperpolarizing fluorescence (~19 ms) (Figure 6).

Figure 7 shows a representative experiment with TMR6M on oocytes expressing T460C to illustrate the method. Figure 7A shows the fluorescence trace in response to the voltage jump protocol (voltage waveform displayed above) when the oocyte was labeled in Na buffer. Depolarizing the membrane resulted in an increase in fluorescence (red trace), which reversed when the membrane potential returned to the holding potential. Hyperpolarizing the membrane resulted in a decrease in fluorescence (black trace). The magnitude of the fluorescence response (ΔF) is the difference between depolarizing and hyperpolarizing fluorescence level at the end of the voltage jump, 7.8 au in this example. When an oocyte expressing T460C was labeled with TMR6M in choline, ΔF was reduced to 4.2 au (Figure 7B), indicating greater accessibility to the 460 residue in the presence of

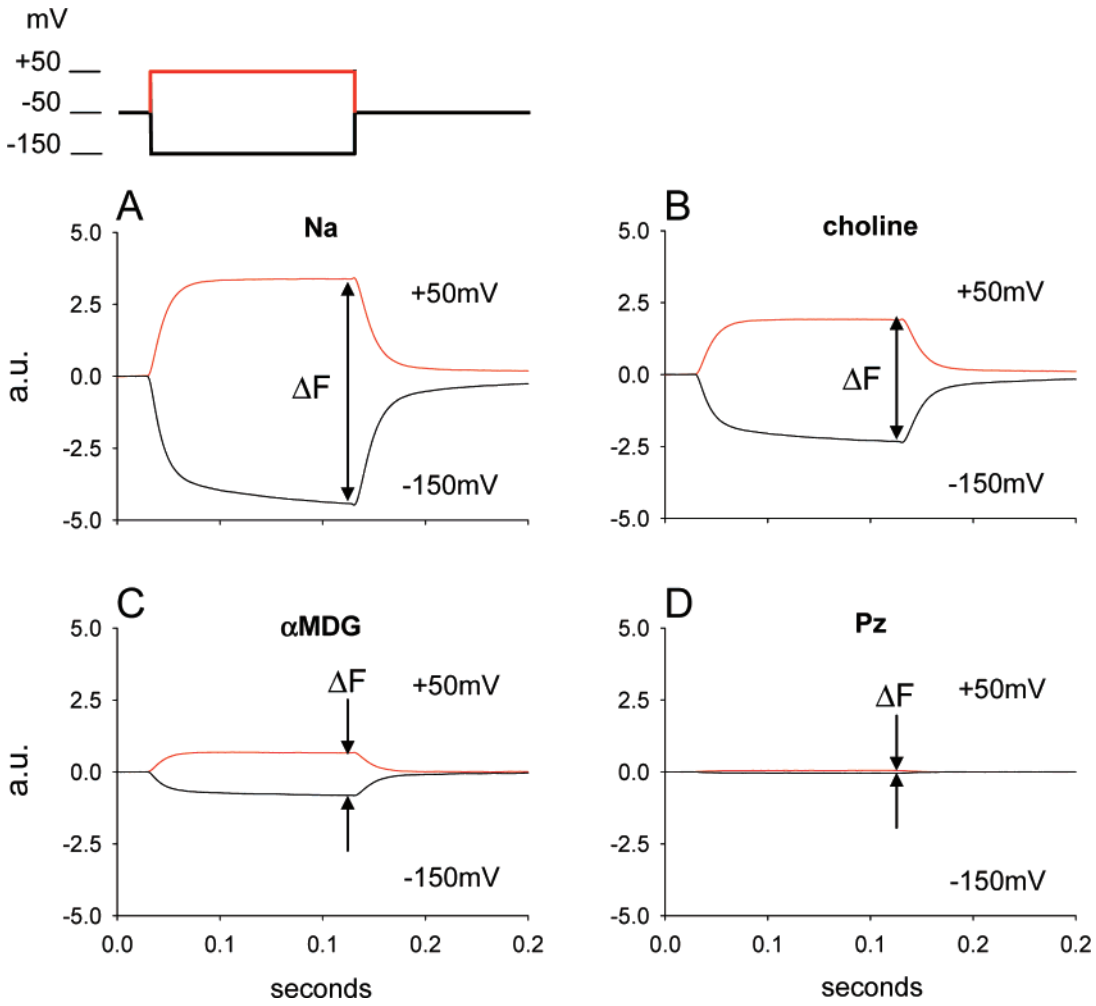

FIGURE 7: Accessibility of Cys mutant T460C to labeling by TMR6M. An example of the method for measuring accessibility to residues on the transporter is illustrated for the T460C hSGLT1 mutant labeled with TMR6M. A single batch of oocytes was labeled with 100 μM TMR6M in Na^+ buffer alone, choline buffer, or Na^+ buffer with either 100 mM αMDG or 500 μM phlorizin for 10 min. Excess dye was then removed by multiple washes with Na^+ buffer, and a representative oocyte was mounted in the VCF chamber. In T460C labeled with TMR6M, the signal in response to the +50 mV pulse (red) is an increase in fluorescence, whereas the −150 mV (black) voltage pulse results in an quench. The largest ΔF (in Na^+) indicates the C2Na conformation was most easily labeled. The mean values are given in Figure 8.

Na^+ compared to its absence. Accessibility was further reduced when the labeling with TMR6M was done in the presence of either substrate (αMDG) or the competitive inhibitor (phlorizin, Pz), ($\Delta F = 1.5$ and 0.1 au, Figure 7C,D). This demonstrated that the rate of labeling of T460C by TMR6M varied by ~80-fold depending on the conformation of the transporter.

This method was applied successfully to seven other Cys mutants (Figure 8). The results fell into three groups: Group 1 (Q457C and Q445C) was more accessible in Na^+ than the other three conditions (Na ≫ Cho, αMDG, Pz), and the results with Q457C were entirely consistent with those reported previously from functional assays (*10*). Group 2 (T460C, G507C, and L527C) was most accessible in Na^+ and least accessible in Pz, but choline and αMDG were intermediate (Na > Cho > αMDG > Pz). Group 3 (I443C, E503C, and Y528C) were most accessible in Pz or αMDG (Pz, αMDG > Na, Cho). Most dramatic was the increase in accessibility of I443C in phlorizin ($C3Na_2Pz$) over the other conformations. Low ΔF values for mutants A439C, A530C, A535C, V542C, and I544C excluded them from this analysis.

Effect of Mutations on Sugar Selectivity. In these experiments we measured the $K_{0.5}$ for D-glucose and for the deoxy sugars in oocytes expressing each cysteine mutant using the two-electrode voltage clamp. The values obtained for D-glucose and αMDG are listed in Table 1. The changes observed in $K_{0.5}^{Glc}$ (0.5 ± 0.1 mM in wild type) were small except for A439C (3 ± 0.4 mM), Q457C (11 ± 1.2 mM), and T460C (1.6 ± 0.3 mM). Likewise, $K_{0.5}^{\alpha MDG}$ increased significantly in A439C, Q445C Q457C, T460C, and A530C by 2−7-fold. These results for D-glucose are displayed graphically in Figure 9, which shows that the glucose $K_{0.5}^{mutant}/K_{0.5}^{wt}$ ratio was increased by more than a factor of 2 for A439C, Q457C, and T460C, suggesting that modifying the protein at these locations adversely affected sugar transport. None of the mutations reduced $K_{0.5}^{Glc}$. Glucose and αMDG were recognized equally by wild-type SGLT1 and most mutants, but the methyl group improved affinity for Q457C (2-fold) and decreased affinity at T460C and A530C (3-fold; Table 1).

The effect of removing the hydroxyl from each position on the pyranose ring was normalized to that for glucose, that

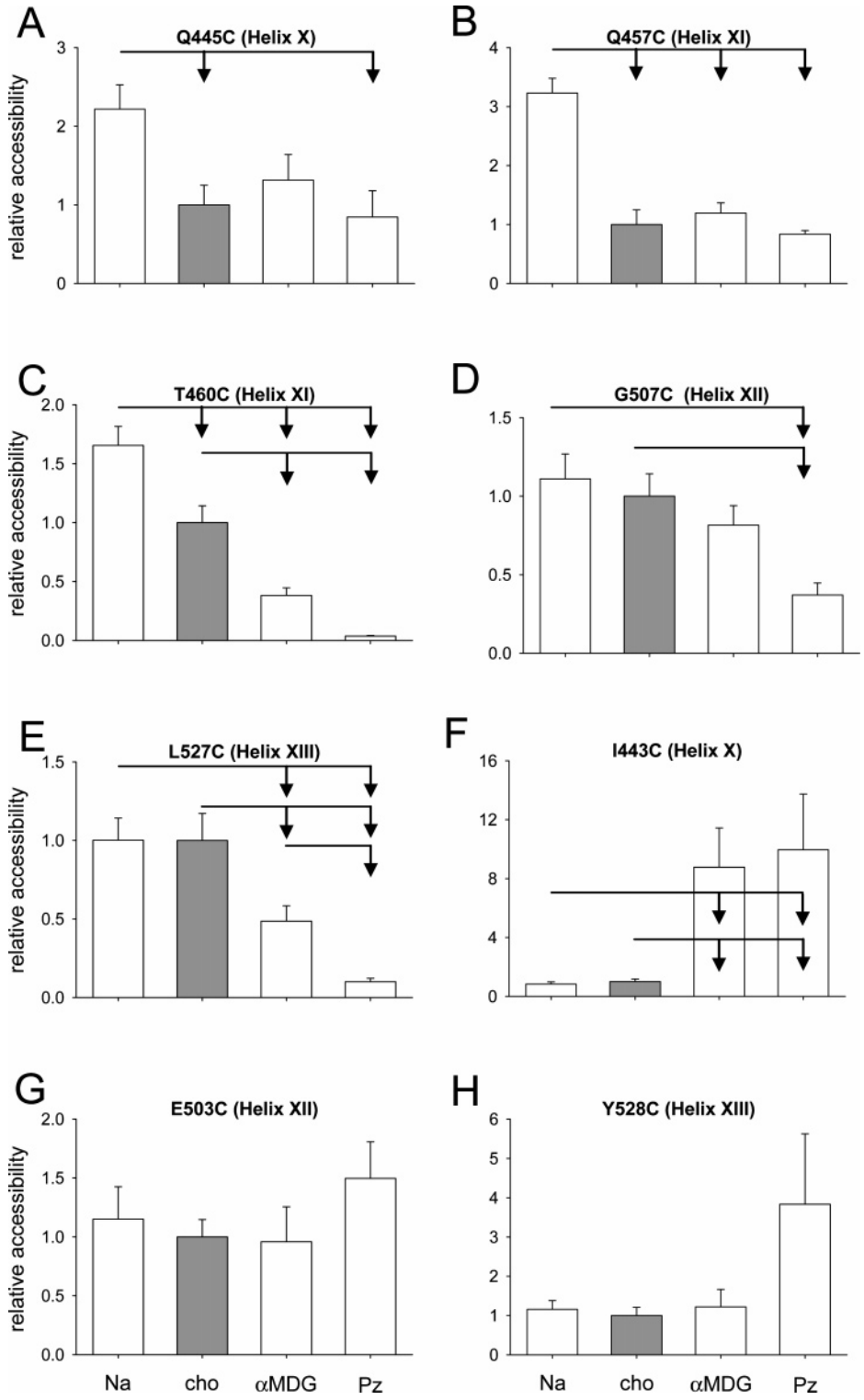

FIGURE 8: Accessibility patterns of hSGLT1 mutants to TMR. Accessibility of eight Cys mutants of hSGLT1 to fluorescent dyes in Na^+ buffer ± sugar or phlorizin, or in the absence of Na^+, is compared as described in Figure 7 for T460C. ΔF after labeling in each condition was normalized to the ΔF measured for labeling in choline. Analysis of variance indicated significance in accessibility in all mutants, except E503C and Y528C, at the 0.01 level. Significant differences within each group were tested with the TukeyHSD test (0.05 level), from the condition at the origin of the line as indicated by the arrows. Data are the mean ± SEM for 4−15 oocytes for each mutant and condition. TMR6M labeling was used for I443C, Q445C, Q457C, T460C, and G507C. E503C, L527C, and Y528C were labeled with TMR-MTS.

is, $K_{0.5}^{deoxy}/K_{0.5}^{Glc}$. Because of the variability of the results, a factor of 2 difference was the minimum change in the ratio that we consider as significant (solid bars). The results for 1-deoxyglucose in Figure 9 (1DOG) show that removal of the 1-OH reduced the apparent affinity of A439C, Q445C, Q457C, and T460C for the sugar but did not increase the apparent affinity in any mutant. In contrast, the $K_{0.5}^{4DOG}/K_{0.5}^{Glc}$ ratio increased for A439, Q457, and T460 and decreased for A468C, E503C, L527C, and Y528C (Figure 9, 4DOG). Ten of the 15 mutants showed increased ratios

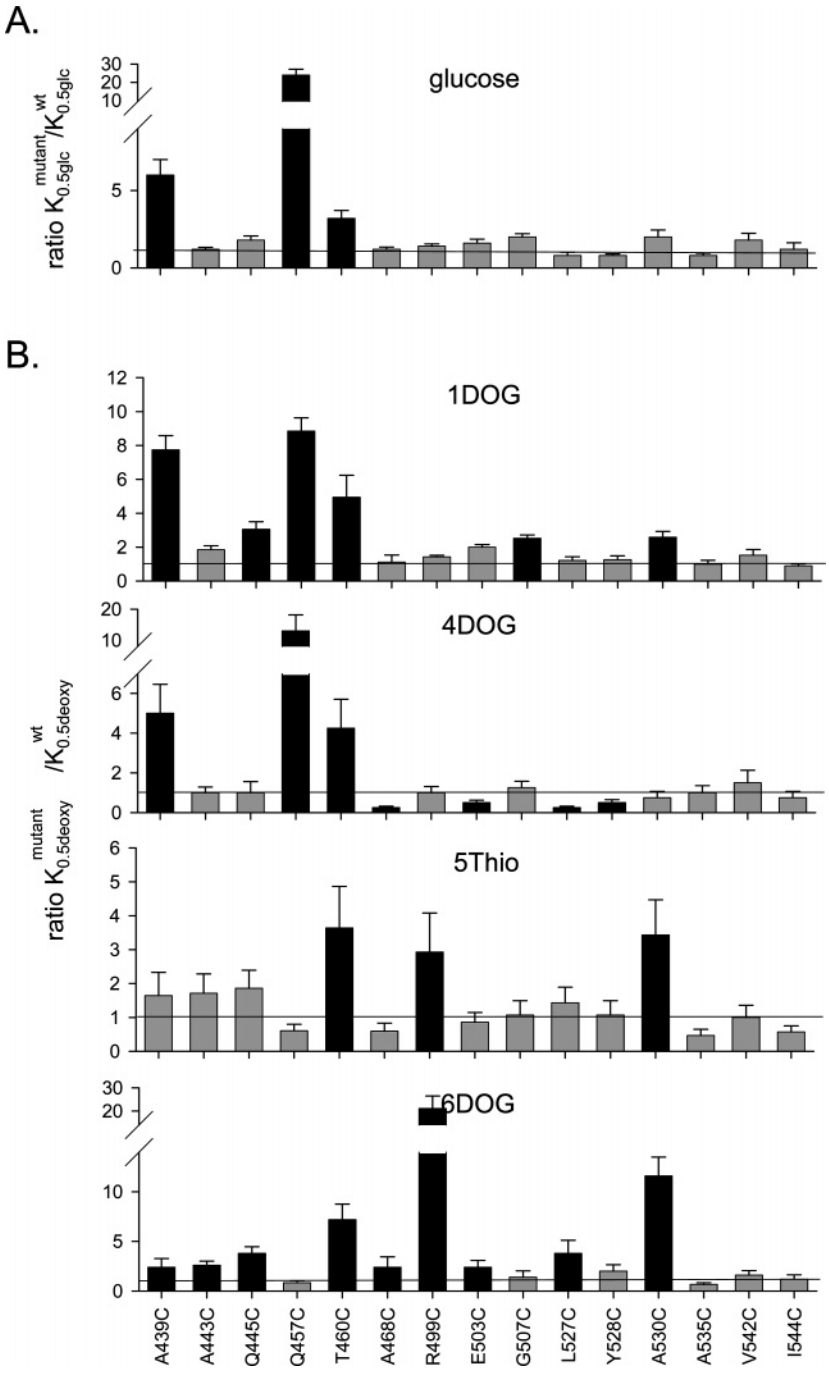

FIGURE 9: Sugar specificity of Cys mutants. The effect of replacing the native amino acid by Cys on sugar specificity was compared at 15 different positions. For glucose the $K_{0.5}^{Glc}$ for each mutant was compared to the $K_{0.5}^{Glc}$ for the wild type ($K_{0.5}^{mutant}/K_{0.5}^{wt}$). For each deoxy sugar in a given Cys mutant, the ratio is normalized to $K_{0.5}^{Glc}$ ($K_{0.5}^{DOG}/K_{0.5}^{Glc}$) for that mutant. The horizontal line is at a value of 1, in which there was no change in $K_{0.5}$ of the deoxy sugar compared to glucose. Black bars designate changes greater than a factor of 2. A change in $K_{0.5}$ resulted from deletion of the -OH at each position of the pyranose for the wild-type hSGLT1. By use of the single concentration estimate, $K_{0.5}^{Glc} = 0.5 \pm 0.1$ mM; $K_{0.5}^{1DOG} = 19 \pm 1$ mM; $K_{0.5}^{2DOG} = 150 \pm 21$ mM; $K_{0.5}^{3DOG} \gg 100$ mM; $K_{0.5}^{4DOG} = 0.4 \pm 0.1$ mM; $K_{0.5}^{5Thio} = 14 \pm 4$ mM; and $K_{0.5}^{6DOG} = 5 \pm 0.7$ mM). These estimates were within a factor of 2 of those values obtained from the full kinetic analysis.

with 6DOG, but the largest values were for A439C, T460C, R499C, and A530C (Figure 9, 6DOG). A different pattern was recorded for 5-thioglucose, where increased ratios were observed for A439C, T460C, and A530C (Figure 9, 5Thio). There were no increases in affinity, reduction in $K_{0.5}^{deoxy}/K_{0.5}^{Glc}$, for 5Thio or 6DOG. This analysis could not be applied to 2DOG and 3DOG as those substrates were poorly recognized by wild-type and all mutant SGLT1s ($K_{0.5} \gg 100$ mM).

DISCUSSION

In this study we have used a SCAM approach, combined with functional characterization of Cys mutants, to map ligand-induced conformational changes underlying Na/glucose cotransport and identify residues involved in sugar binding. Previously, we have located the sugar binding and translocation domain of hSGLT1 to transmembrane helices (TMH) X−XIV (*1*−*3*). We have focused on TMHs X−XIII,

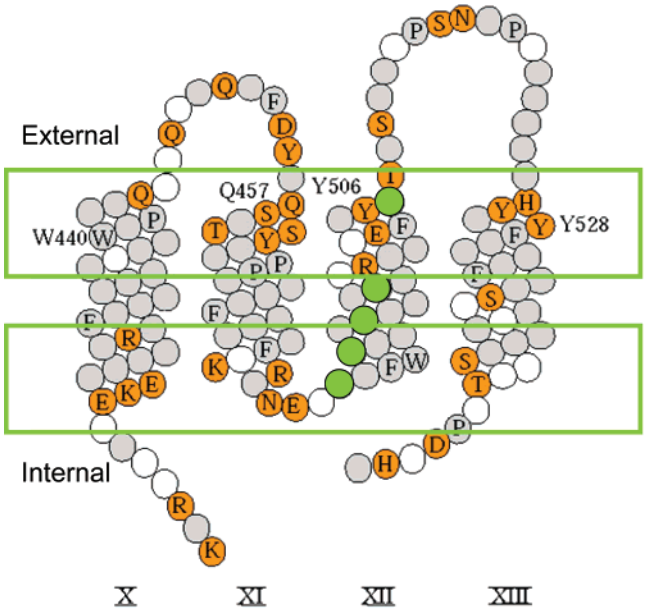

FIGURE 10: Sequence comparison of SGLT family transporters TMH X−XIII. The amino acid sequence of TMHs X−XIII of the SGLT transporters is highly conserved. Conserved residues that have a high propensity for participation in sugar binding are named and highlighted in orange. These include charged and polar residues that can interact with the sugar hydroxyls, and aromatic residues that participate in characteristic stacking interactions with the pyranose ring, particularly Trp and Tyr. The charged, polar, and aromatic residues are mostly located near the helix ends. Only one charged residue, R499, is well within the membrane and we propose that this forms a salt bridge with E503, one turn higher on TMH XII. The green squares outline the regions that comprise putative internal and external sugar binding sites. Small hydrophobic residues (G, A, V, L, conserved) are gray, except for the periodic motif of glycine (green) on TMH XII, which may indicate a site of close helix−helix contact. Open circles designate nonconserved residues. The two- or three-residue linker (NEP/QK) between TMHs XI and XII requires that these helices be closely associated. TMHs X and XI are linked by a 10-residue hydrophilic loop (XQSGQLDX), and TMHs XII and XIII by a 17-residue loop [TGSCXE(QRA)PSN-(AS)CPT(KAQ)XXSXV, where X is a nonconserved residue]; both are highly conserved in the 30 SGLTs. There are three helix-breaking proline residues, one near the external end of TMH X and two adjacent near the middle of TMH XI.

as TMH XIV is missing in several members of the SLC5 gene family and is probably not essential for function. One aspect of the topology of SGLT1 that has yet to be fully resolved is whether or not the cytoplasmic loop between TMHs XIII and XIV (Figure 1) forms a reentrant loop into the plasma membrane (see *25*, *26*). As yet, there is no evidence that such a putative reentrant loop is directly involved in sugar binding or translocation. Figure 10 summarizes the conservation in primary amino acid sequence overlaid on the topological model of TMHs X−XIII. Analysis of the conserved residues in 22 sugar transporters in 30 mammalian members of the SLC5 gene family reveal that only 14 of the 128 residues within TMH X−XIII are not conserved (open circles): nine in the TMH domains and five in the hydrophilic linkers between the helices. The gray residues are conserved, small, hydrophobic side chains (G, A, V, L). Charged or polar residues are orange, and residues with a high propensity for interaction with sugars are identified. Four glycine residues located along one face of TMH XII are conserved in all SLC5 sugar transporters, suggesting a close relationship to another TMH (*27*). There are three proline residues, one near the external end of TMH X and two adjacent near the middle of TMH XI. These produce kinks in TMHs X and XI, and we speculate that this flexibility is important in the ligand-induced conformational changes that occur during the Na/sugar transport cycle.

Our proposal is that faces of TMHs X−XIII form a hydrophilic pocket on the external face of SGLT1 that comprise an external sugar binding site (Figure 11). Experiments on the cytoplasmic side of SGLT1 indicate a second internal sugar binding site (*28*, *29*). The three-residue linker (NEX, where X is nonconserved) between TMHs XI and XII is a structural constraint that requires these helices be closely associated. TMHs X and XI are linked by a 10-residue hydrophilic loop, and TMHs XII and XIII by a 17-residue loop (*20*, *21*).

We identify three residues that we propose are directly involved in glucose binding and translocation from the external solution, three more that face the binding site, and eight residues not expected to bind sugar but that affect sugar recognition, possibly by distorting the binding site. In addition, access to nine residues on TMHs X− XIII is dependent on protein conformation.

We will consider and discuss the effects of the new Cys mutants relative to those of Q457, and present the data in two sections: first, how SGLT1 conformation changes accessibility of each mutant to the external environment, and second, the functional effect of changing the residue to Cys; and then we will integrate these data to postulate an external sugar binding-site structure.

Conformational Effects on Accessibility. When Q457C is derivatized with MTS reagents, transport is abolished (*9*, *10*), and we have previously shown that Q457 is exposed to the external environment only in the Na-bound state ($C2Na_2$, Figure 2, *10*). Our explanation is that when Na binds, a conformational change is induced that results in the sugar binding site opening to the external environment, the $C2Na_2$ conformation, and those residues facing the sugar binding pocket become accessible to external labeling reagents. Occupying the binding site with phlorizin ($C2Na_2Pz$) physically restricts access to those residues. In the presence of sugar the transporter is predominantly in $C5Na_2$ (or C6) and the external binding site is closed to external access (Figure 2; refs *6* and *10*). We used these criteria as a basis for comparing the characteristics of the other residues in this study.

MTS reagents also blocked transport by T460C, A468C, and R499C, and we observed a similar pattern of MTS accessibility to that for Q457C, suggesting that they line the hydrophilic cavity forming the sugar binding site (see below). Even in the $C2Na_2$ conformation, access to A468C and R499C was restricted, as they were only labeled by the smallest MTS reagents (MeMTS), whereas the larger TMR6M and TMR-MTS did not label these residues in any conformation. These observations suggest a constriction in the sugar pathway.

Glucose transport by I443C was blocked by MTS reagents (Figure 3B and Table 2), but accessibility to these compounds was highest in the presence of phlorizin ($C2Na_2Pz$) and sugar ($C5Na_2$), suggesting I443C is not facing the sugar binding site (Figures 3B and 8F). A439, one turn deeper into the

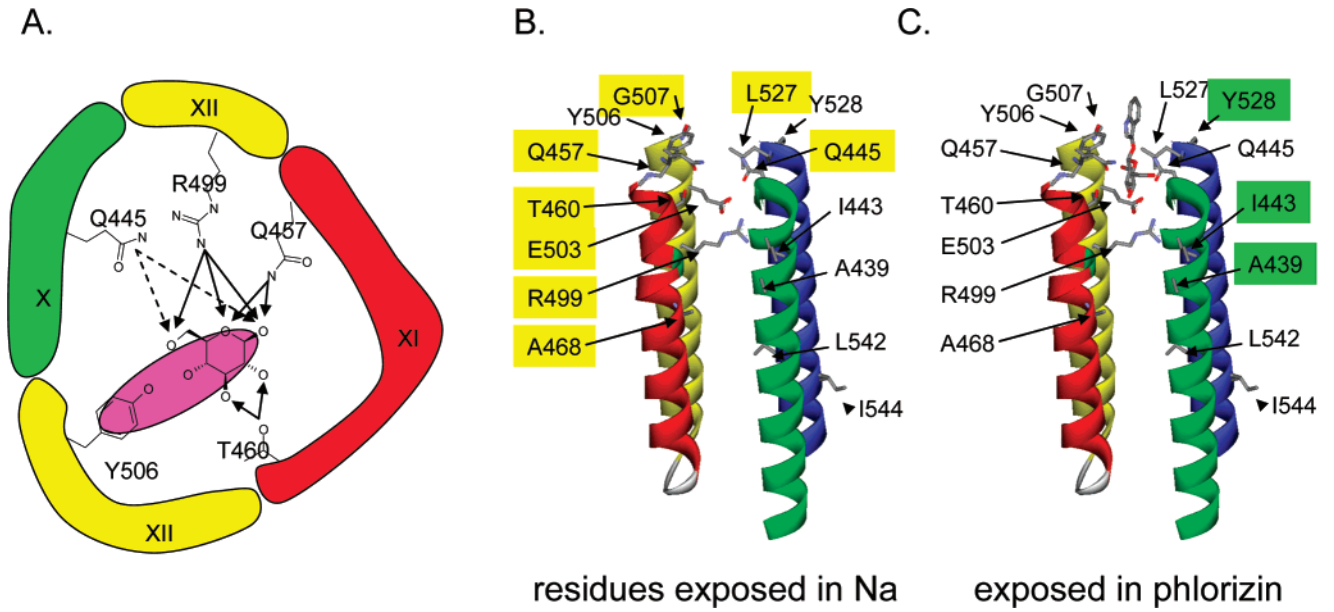

FIGURE 11: Model of the sugar domain of hSGLT1. (A) Schematic of proposed interactions with glucose. We speculate that the sugar binding site includes residues Q445, Q457, T460, R499, and Y506. The arrows indicate interactions with sugar hydroxyls; solid lines are proposed to be direct interactions, while dashed lines signify weaker interactions, possibly mediated via water. The magenta shape indicates aromatic stacking with the hydrophobic surface of the pyranose. Helical identification corresponds to panel B: TMH X is green, TMH XI is red, TMH XII is yellow, and TMH XIII is blue. (B) Three-dimensional model, displaying the mutated residues as sticks. We have also included Y506. Q445, Q457, Y506, and A530 are oriented to face the sugar pathway; I443 and Y528 are directed away from the pathway. A530 and A535 are not visible. Residues exposed to the external environment in conformation $C2Na_2$ are shown with yellow labels. (C) Residues exposed to the external environment in conformation $C7Na_2Pz$ are shown with green labels.

membrane, was insensitive to MTS reagents, but this may simply be due to poor access by small MTS reagents (Table 2).

We determined the effect of conformation on accessibility of those cysteine mutants where there were no functional effects of MTS by using a new fluorescent dye binding assay. The validity of the assay was confirmed with Q457C where we found that access of this cysteine to TMR6M was high in the presence of Na and significantly reduced when sugar or phlorizin was added, or in the absence of Na (Figure 8B). This is in complete agreement with the results obtained for the inhibition of Na/glucose cotransport by MTS reagents (*10*). Similar results to those with Q457C were observed with Q445C and T460C (Figure 8A,C), while only the presence of sugar and phlorizin significantly reduced TMR binding to G507C and L527C (Figure 8D,E). This leads to the conclusion that the addition of Na^+ to the external medium opened up access to residues Q445 (TMH X) and Q457 and T460 (TMH XI), and the further addition of transported sugar, or the nontransported blocker phlorizin, reduced access to Q445 (TMH X), Q457 and T460 (TMH XI), G507 (TMHXII), and L527 (TMH XIII).

In contrast, the presence of phlorizin or sugar in Na buffer dramatically increased access of TMR to I443C, indicating that in conformations $C7Na_2Pz$ and $C3Na_2S$ I443C is exposed to the external environment. Recalling that in these conformations Q445C, located on the opposite side of TMH X, is not accessible from the outside suggests that TMH X undergoes motions that alternately expose these two sides of the helix to the external mileu. The effects of phlorizin on TRM accessibility to Y528C and L527C suggest a similar alternating exposure at the tip of TMH XIII (Figure 8E,H). Collectively, these binding studies point to sodium opening, phlorizin blocking, and sugar closing the sugar binding pocket between helices X, XI, XII and XIII. E503C, between G507 and R499, was equally accessible in all conformations (Figure 8G).

We note that transport of sugar is coupled to the stoichiometric influx of Na^+, which depolarizes the membrane. For a membrane potential of −50 mV under saturating concentrations of Na and sugar, as achieved by use of the voltage clamp, the predominant conformation is $C5Na_2$. If the membrane potential is not controlled, the membrane will depolarize and the C6 state becomes increasingly abundant. Therefore, in the labeling experiments with TMR in the presence of sugar, where we did not control of the membrane potential, $C5Na_2S$ may not be the predominant conformation, depending on the level of functional expression of a mutant. Addition of phlorizin to the Na buffer does not significantly alter the membrane potential, and so the predominant conformation is $C7Na_2Pz$. Our identification of residues exposed to the external environment in the $C2Na_2$ conformation, and not in other conformations, remains valid.

Interactions with Sugar. Structural studies of sugar binding proteins have shown that polar planar side chains (Asn, Glu, Asp, Gln, Arg, and His) interact via H-bonds with the sugar hydroxyls, and there is also a characteristic stacking of the hydrophobic face of the pyranose ring with Trp or Tyr (*30*−*32*). Figure 10 highlights the residues that have a high propensity to occur in sugar binding sites. Note that there are two clusters of residues, one at the extracellular surface and another at the intracellular surface of the protein. Here we focus on residues at or near the putative external sugar binding site. Changing residue T460 to Cys decreased the affinity for D-glucose (Table 1) and altered sugar selectivity (Figure 9), similar to Q457C. The $K_{0.5}^{Glc}$ of R499C was

unaffected, but this mutation did alter sugar recognition strongly at the pyranose 6-position (Figure 9), suggesting a role in sugar recognition.

Accessibility of Q445 (Figure 8A) strongly suggests that it faces the sugar binding site, but its interaction with the sugar is not clear. We observed only subtle effects on glucose affinity and sugar selectivity with Q445C (Table 1 and Figure 9); there was no change in glucose affinity and modest decreases in αMDG and 6DOG affinity. In addition, MTS reagents did not inhibit transport; Q445C should be labeled since the cysteine is accessible to the large dyes (see Table 2). Large reagents (TMRM6) blocked transport, due probably to steric effects.

Small and/or nonpolar side chains (Ala, Gly, Ile, and Leu) are not expected to participate in sugar binding but there is evidence that A468C, L527C, and A530C affect the binding site as these cysteine mutations produce clear functional effects. This may be a reflection of the change in bulk of the side chain (*33*) or charge if the Cys is ionized to a thiolate. The A468C mutation resulted in a subtle shift in sugar selectivity: $K_{0.5}$ for 5-thioglucose was reduced 5-fold while that for 6DOG was increased 2-fold compared to wild type (Figure 9). Cysteine mutations at L527, G507, and A530 produced a relatively specific loss in affinity for 6DOG (Figure 9) without introducing sensitivity of glucose transport to MTS labeling. At least for G507C and L527C, the lack of effect of MTS was not due to inaccessibility, as both were labeled with TMR6M (Figure 8). There was no change in sugar affinity or selectivity of I443C (Table 1 and Figure 9). Although the affinity for glucose of A439C (one helical turn deeper into the membrane from I443) was reduced 5-fold (Table 1) and there was a dramatic change in sugar selectivity (Figure 9), Ala is also not likely to be a sugar binding residue, and so this may be due to increased size of cysteine causing a shift in the arrangement of the helices or in the presence of the thiolate anion.

Structural Model. We built the model of transmembrane helices X−XIII based on our data and secondary structure model (Figure 10; *20*, *21*). Our SCAM results (Figure 8) indicate that in the $C2Na_2$ conformation Q445 (TMH X), Q457, T460, A468 (TMH XI), R499, E503, G507 (TMH XII), and L527 (TMH XIII) face or have an exposure to the sugar pathway. I443 (TMH X) and Y528 (TMH XII) do not face the sugar pathway. We also note that R499 and E503, on the same face of helix XII and one helical turn apart, could form a salt bridge. A simple computational chemistry calculation on helix XII [Hyperchem v 6.03 (Hypercube, Gainesville, FL) Amber force field, in vacuo) confirmed this possibility (unpublished observations). If the secondary structure model is correct, there are no other side chains in similar positions in these helices that can interact via an ionic interaction with either E503 or R499. We integrated these results with the effects on sugar specificity of mutations at these and five additional sites to construct a model of the sugar binding domain (Figure 11).

Rationale for the Structure. Clues about the nature of the sugar binding site come from the selectivity of hSGLT1 (Table 1; *9*, *23*). Only hexoses with equatorial -OH groups on C2 and C3 are transported with high affinity. 2-Deoxy-2-amino-D-glucose (glucosamine), 2-fluoro-2-deoxy-D-glucose, D-mannose, and D-allose are poor substrates ($K_{0.5} \gg$ 100 mM; *9*), indicating a precise arrangement of hydrogen bonding with the protein. Although 3-deoxy-D-glucose is a very poor substrate ($K_{0.5} \gg$ 100 mM, *34*), both 3-*O*-methyl-D-glucose and 3-*O*-benzyl-D-glucose are accepted ($K_{0.5} = 6$ and 30 mM, *9*; J. M. Planas and E. M. Wright, unpublished results), demonstrating the existence of an H-bond between the protein and the equatorial oxygen at C3. 1-, 4-, and 6-deoxy-D-glucose are all transported with $K_{0.5} < 10$ mM, demonstrating that H-bonding with any one of these single -OH groups is not essential. A constrained dipole interaction at the 4-position was proposed on the basis of the observation that 4-fluoro-4-deoxy-D-glucose is a high-affinity substrate (*9*) but 4-fluoro-4-deoxy-D-galactose is not (0.07 vs 1.7 mM, *34*). Although the 6-OH is not essential, C6 may be important in hydrophobic interactions, as D-xylose has a $K_{0.5} >$100 mM (*9*). The pyranose ring -O- may be replaced with -S- but not -NH- or $-CH_2-$ (*9*, *34*). Glucopyranosides, including those with aliphatic chains, phenyl, naphthyl, and indoxyl groups are transported but only as the β anomer; thus, the aromatic rings must lie in the same plane as the pyranose ring; for example, indican is transported with a $K_{0.5}$ of ∼0.1 mM (*23*, *35*).

Taken together, these observations indicate that the sugar binding site positions the pyranose ring so that: (1) the 1-OH points out of the binding site, and the vestibule open only in the direction of the β-OH; (2) the 2-OH faces a rigid array of H-bond donors and acceptors; (3) the equatorial 3-OH faces a large space, containing in the aperture a precisely placed H-bond donor; (4) a dipolar interaction instead of H-bonding probably occurs at the 4-OH; (5) the pyranose oxygen accepts an important H-bond(s) but the binding site cannot accommodate a donation from an amide in the 5-position; and (6) a hydrophobic interaction with C6 is suggested by the affinities of 6DOG and D-xylose.

Q457, as noted above, is on TMH XI, in the sugar binding site, and SCAM has shown its exposure as a function of substrate and membrane potential is consistent with an alternating access model of cotransport: Q457C is accessible to labeling with Cys-specific MTS reagents only in the Na-bound ($C2Na_2$) conformational state (*10*), establishing that when Na is bound the sugar binding site is open to the external solution. This is consistent with the increase in sugar affinity upon addition of external Na (*14*). There was no electrophoretic effect of labeling with charged MTS reagents, in contrast to A468C, consistent with its placement at the extracellular end of TMH XI (*10*).

We observed the largest change in $K_{0.5}{}^{Glc}$ for Q457C (0.5 mM in wt to 12 mM in Q457C, for a $K_{0.5}{}^{Q457}/K_{0.5}{}^{wt} = 24$; Figure 9), consistent with the key role this residue plays in transport, and a large difference between the $K_{0.5}{}^{1DOG}$ between wt and Q457 ($K_{0.5}{}^{Q457}/K_{0.5}{}^{wt} = 9$; Figure 9). We also measured a large increase in $K_{0.5}$ for 4DOG, but there was no difference in the $K_{0.5}$ values of 4DOG, glucose, and galactose in the wild-type transporter. This indicates that the 4-OH is not essential for sugar recognition. We propose that the increased $K_{0.5}{}^{4DOG}$ is an indirect effect of the loss of H-bonding to 1-OH and 5-O- when Gln was replaced by Cys.

Q445, on TMH X, has the same accessibility characteristics as Q457 (Figure 8A) and so is placed facing the sugar, an orientation compatible with the placement of I443 facing away from the sugar pathway. Its estimated reactivity rate for TMR6M labeling is also similar to that of Q457C (Table

2), and the polarity of the fluorescence (depolarizing voltage quenches the fluorescence, Figure 6) indicates it undergoes a similar environmental change as the conformation changes from $C2Na_2$ to C6. Functionally, Q445C sugar specificity suggests interactions with 1-OH and 6-OH, which may be via water intermediates, as the changes in $K_{0.5}$ are modest compared to Q457C and only large Cys reagents block transport.

G507 accessibility to labeling, at the top of TMH XII, was blocked in the presence of phlorizin (Figure 8D), and so in our model G507 was oriented to face the sugar pathway. It is not expected to make a side-chain interaction with the sugar, although it is possible that the effect is due to increased bulk of the Cys, a change in charge if the Cys is ionized, or disruption of a sugar−backbone interaction. The greatest influence of the G507C mutation was at the pyranose 6-OH.

L527 labeling (TMH XIII) was blocked by sugar and phlorizin (Figure 8E), and so it is also likely to face the sugar pathway. The rate of labeling of L527C by TMR-MTS was an order of magnitude less than E503 (Table 2), indicating that it is in a comparatively restricted space and further suggesting that the effect of L527C on sugar specificity may be the result of an alteration of binding-site structure due to a change in the bulk of the side chain. Its greatest influence on sugar specificity, like G507C, was an increase in the estimated $K_{0.5}$ for 6DOG and a decrease in $K_{0.5}$ for 4DOG.

T460 is one helical turn below Q457 and has the same estimated reaction rate to TMR6M as Q457C (Table 2), suggesting that, even though it is deeper into the membrane, in the $C2Na_2$ conformation it has the same exposure to the extracellular solution as Q457C. The fluorescence signal, however, is opposite in polarity to Q457C, increasing in intensity with depolarization as the protein goes from the $C2Na_2$ to C6 conformations (Figure 6). This suggests that in C6 the dye is experiencing an environment near T460 that is different than that experienced near Q457; deeper in the protein, the dye may be sensing the amino acids in the binding site, compared to the aqueous external mileu sensed by the surface-exposed dye linked to Q457C. From its proximity to Q457, T460 could be expected to make specific interactions with the sugar, but instead mutation to Cys caused a general increase of $K_{0.5}$ at all positions (Figure 9).

A468 side chain is unlikely to interact with the sugar, consistent with the A468C mutation having no effect on the $K_{0.5}$ for glucose and a small effect on sugar specificity at 6-OH (Figure 9). Apparent affinity increased for 4DOG, but an explanation for this effect awaits further study. Alkylating A468C with MTS reagents completely stopped transport, suggesting that this residue is involved in the transport process. This residue is in a sterically restricted area about halfway through the membrane (see Figure 5), as only the small MTS reagents had access: we could not label it with either TMR6M or TMR-MTS. A468C, three helical turns below Q457 in the model, faces the sugar pathway, and as it is only accessible in the Na-bound conformation (Figure 3A), an integration of the results from this face of TMH XI suggest that it forms one side of a cuplike vestibule, open to the outside in conformation $C2Na_2$, followed by a constriction at position 468.

R499 is two helical turns below G507 on TMH XII and was only accessible to labeling in the presence of Na, consistent with an orientation in the sugar pathway. It is, however, in an even more restricted space than A468, since only the smallest MTS reagent, MeMTS, had access. Both G507C and E503C (discussed below) were accessible to labeling with the dyes (Figure 8D,G), indicating they are exposed in a vestibule, but by the next helical turn, position 499 is in a tightly packed environment. It is a potential sugar-binding residue with its largest effect on pyranose 6-OH.

E503 is on the same face of TMH XII as R499 and G507; however, this position did not have a strong conformational dependence on accessibility to labeling by the dye (Figure 8G). There was also no large effect on substrate selectivity, suggesting no strong interaction with the sugar (Figure 9). E503C was labeled by TMR-MTS, indicating that E503 is in a space easily accessible to the large dye. It had no preferred conformation for labeling, whereas both R499C and G507C were least accessible in the phlorizin-bound conformation. These characteristics also suggests a cuplike vestibule formed by this face of TMH XII, followed by a region of close helical packing, similar to TMH XI.

The possibility that R499 and E503 are salt-bridged begs additional experiments to explain to some important observations. Both mutants R499C and E503C are fully functional, suggesting that the salt bridge is not essential for function. Sugar recognition by R499C for 1DOG, 5Thio, and 6DOG is altered severalfold more than it is by substituting Cys in E503 (Figure 9). This may be explained if loss of the Arg disrupts sugar recognition in R499C, and the thiolate anion in E503C is able to form a salt bridge with R499. However, there was no effect on $K_{0.5}$ for glucose in either mutation.

I443 (TMH X) is certainly not in the sugar pathway from SCAM, being highly accessible to labeling by the dyes in the phlorizin- or sugar-bound ($C7Na_2Pz$ or $C5Na_2$) conformations (Figures 3B and 8F). In addition, a helical structure places it on the opposite side from Q445, so the effect of the Cys mutation on recognition of 6DOG must be indirect, i.e., from a distortion of the binding site. It is very accessible in the phlorizin-bound conformation, which suggests that in both the $C2Na_2$ and C6 conformations I443C is shielded from the external environment. Despite this, the fluorescence signal between the depolarizing (C6) and hyperpolarizing ($C2Na_2$) conformations (Figure 6) suggests this transition involves a change in the environment around residue I443.

A439, one turn below I443, was difficult to label (Table 2), suggesting a tight packing environment under all substrate conditions. The side chain is not expected to interact with the sugar, so the increased $K_{0.5}$ at all positions of the sugar ring suggests that the Ala → Cys mutation results in a distortion of the sugar binding site from a displacement of TMH 10 and deformation of the sugar binding site.

Y528 accessibility suggests that it is not in the sugar binding site, since it is labeled by TMR-MTS in the presence of phlorizin (Figure 8H), consistent with a location on the face of TMH XIII away from the sugar pathway. The reaction rate of labeling Y528C with TMR-MTS was an order of magnitude lower than for this dye for L527C, suggesting Y528 is in a more confined space (Table 2). We consider the effect on recognition of 4DOG nonspecific.

A530 is one helical turn below L527, and the side chain is not expected to interact with the sugar. It is located at about the same level (in the model) as E503, but its difficulty in labeling also suggests it is not facing the sugar pathway

but is in a region of restricted access. We suggest that the effect of the mutation to the larger Cys on sugar recognition is a distortion of the binding site or an effect of a thiolate anion.

The remaining mutants, A535C, V542C, and I544C were inaccessible to the dye, consistent with being both deeper in the membrane and past a constriction in the sugar pathway. None showed any significant functional effects.

Summary. Integrating these results leads us to a 3-D structural model of the external sugar binding domain of hSGLT1 (Figure 11). TMHs X−XIII are arranged in a clockwise sequence (viewed from the extracellular side). Upon binding Na, the conformation of SGLT1 changes from empty (C6, C1) to the $C2Na_2$ conformation (Figure 2), and the three faces of TMHs X, XI, and XII, defined by Q445 (X), Q457, T460, and A468 (XI), and G507, E503, and R499 (XII), form an outward-opening vestibule that constricts at A468 and R499. The conformational changes implied in the transport mechanism may be involved in flexibility of these helices at P442 (TMH X) and P465 and P466 (TMH XI). A535 is at the level of A468 and R499 and may also be at the constriction. I443 and A439 are facing away from the sugar pathway. In this arrangement, Y506, which we have not yet studied, is placed in a position to interact with the sugar through the aromatic stacking interaction characteristic of sugar binding sites. We speculate that if the Cys at position 527 is in the thiolate form, it would reduce hydrophobic interaction with the methyl group of 6DOG or disrupt binding by introducing a charge. The contributions of other potentially interacting residues on TMH XIII, H525 and Y526, also remain to be tested. Our study does not preclude ligand-induced conformational changes in other domains of SGLT1 such as that reported for the external hydrophilic loop between TMHs VIII and IX on the basis of atomic force microscopy (*26*).

The charged, polar, and aromatic residues are mostly located near the helix ends. Homology and location on the model suggest residues Y506 and Y526 as possible sugar-binding residues, but there are several other attractive candidates, including W440, S458, Y462, and H525. Only one charged residue, R499, is well within the membrane and we propose that this forms a salt bridge with E503, one turn higher on TMH XII. Other salt bridges may be formed between pairs of charged residues at the cytoplasmic ends of TMHs X and XI.

We have proposed a working model of the helical packing of the sugar binding and translocation domain in the $C2Na_2$ conformation and are working to test it while waiting for the crystal structure to be solved. The binding site is incomplete in that the interactions with 2-OH and 3-OH of the pyranose and the characteristic aromatic stacking have yet to be identified. Our data and the analysis of conserved residues in the sugar transporter family point to two substrate binding sites, one on the external face and the other on the internal face of the protein (Figure 10). A two-binding-site model raises an intriguing question about the translocation of large sugar substrates from one site to the other. The crystal structures of cotransporters obtained so far (*32*, *36*, *37*) show substrate binding sites are deep in the membrane and this suggests different structural solutions to the problem of cotransport or, for example, that the crystal structure is a stable intermediate step in the transport cycle. We look forward to having crystal structures of SGLTs and challenging them with functional data.

ACKNOWLEDGMENT

We gratefully acknowledge expert technical support from Teresa Ku, Patti A. Young, Amanda Johnson, and Hang Nguyen. We also thank Drs. Monica Sala-Rabanal and Andy Voss and Charles Hummel for critical comments on the manuscript.

REFERENCES

1. Panayotova-Heiermann, M., Loo, D. D.F., Kong, C. T., Lever, J. T., and Wright, E. M. (1996) Sugar binding to Na^+/glucose cotransporters is determined by the carboxyl-terminal half of the protein, *J. Biol. Chem. 271*, 10029−10034.
2. Panayotova-Heiermann, M., Eskandari, S., Turk, E., Zampighi, G. A., and Wright, E. M. (1997) Five transmembrane helices form the sugar pathway through the Na^+/glucose cotransporter, *J. Biol. Chem. 272*, 20324−20327.
3. Panayotova-Heiermann, M., Leung, D. W., Hirayama, B. A., and Wright, E. M. (1999) Purification and functional reconstitution of a truncated human Na^+/glucose cotransporter (SGLT1) expressed in *E. coli*, *FEBS Lett. 459*, 386−390.
4. Parent, L., Supplisson, S., Loo, D. D. F., and Wright, E. M. (1992) Electrogenic properties of the cloned Na^+/glucose cotransporter: II. A transport model under nonrapid equilibrium conditions, *J. Membr. Biol. 125*, 63−79.
5. Guan, L., and Kaback, H. R. (2005) Lessons from lac permease, *Annu. Rev. Biophys. Biomol. Struct. 35*, 67−91.
6. Loo, D. D. F., Hirayama, B. A., Karakossian, M. V., Meinild, A.-K, and Wright, E. M. (2006) Conformational dynamics of hSGLT1 during Na^+/glucose cotransport, *J. Gen. Physiol. 128*, 701−720.
7. Virkki, L., Murer, H., and Forster, I. C. (2006) Voltage clamp fluorometric measurements on a type II Na^+-coupled Pi cotransporter: shedding light on substrate binding order, *J. Gen. Physiol. 127*, 539−555.
8. Sala-Rabanal, M., Loo, D. D. F., Hirayama, B. A., Turk, E., and Wright, E. M. (2006) Molecular interactions between dipeptides, drugs and the human intestinal H^+-oligopeptide cotransporter (hPepT1), *J. Physiol. 574*, 149−166.
9. Díez-Sampedro, A., Wright, E. M., and Hirayama, B. A. (2001) Residue 457 controls sugar binding and transport in the Na^+/glucose cotransporter, *J. Biol. Chem. 276*, 49188−49194.
10. Loo, D. D. F., Hirayama, B. A., Gallardo, E. M., Lam, J. T., Turk, E., and Wright, E. M. (1998) Conformational changes couple Na^+ and glucose transport, *Proc. Natl. Acad. Sci. U.S.A. 95*, 7789−7794.
11. Martin, M. G., Lostao, M. P., Turk, E., Lam, J., and Kreman, M, Wright, E. M. (1997) Compound missense mutations in the sodium/glucose cotransporter result in trafficking defects, *Gastroenterology 112*, 1206−1212.
12. Díez-Sampedro, A., Loo, D. D. F., Wright, E. M., Zampighi, G. A., and Hirayama, B. A. (2004) Coupled sodium/glucose cotransport by SGLT1 requires a negative charge at position 454, *Biochemistry 43*, 13175−13184.
13. Ikeda, T. S., Hwang, E. S., Coady, M. J., Hirayama, B. A., Hediger, M. A., and Wright, E. M. (1989) Characterization of a Na^+/glucose cotransporter cloned from rabbit small intestine, *J. Membr. Biol. 110*, 87−95.
14. Parent, L., Supplisson, S., Loo, D. D. F., and Wright, E. M. (1992) Electrogenic properties of the cloned Na^+/glucose cotransporter: I. Voltage clamp studies, *J. Membr. Biol. 125*, 49−62.
15. Javitch, J. A., Fu, D., Chen, J., and Karlin, A. (1995) Mapping the binding-site crevice of the dopamine D2 receptor by the substituted cysteine accessibility method, *Neuron 14*, 825−831.
16. Pascual, J. M., and Karlin, A. (1998) State-dependent accessibility and electrostatic potential in the channel of the acetylcholine receptor, *J. Gen. Physiol. 111*, 717−739.
17. Meinild, A.-K., Loo, D. D. F., Hirayama, B. A., Gallardo, E. M., and Wright, E. M. (2001) Evidence for the involvement of Ala 166 in coupling Na^+ to sugar transport through the human Na^+/glucose cotransporter, *Biochemistry 40*, 11897−11904.

18. Meinild, A.-K., Hirayama, B. A., Wright, E. M., and Loo, D. D. F. (2002) Fluorescence studies of ligand-induced conformational changes of the Na^+/glucose cotransporter, *Biochemistry 41*, 1250−1258.
19. Thompson, J. D., Higgins, D. G., and Gibson, T. J. (1994) CLUSTAL W: Improving the sensitivity of progressive multiple sequence alignment through sequence weighting, position-specific gap penalties and weight matrix choice, *Nucleic Acids Res. 22*, 4673−4680.
20. Turk, E., and Wright, E. M. (1997) Membrane topology motifs in the SGLT cotransporter family, *J. Membr. Biol. 159*, 1−20.
21. Wright, E. M., and Turk, E. (2004) The sodium/glucose cotransporter family SLC5, *Pflugers Arch. 447*, 510−518.
22. Hirayama, B. A., Lostao, M. P., Panayotova-Heiermann, M., Loo, D. D. F., Turk, E., and Wright, E. M. (1996) Kinetic and specificity differences between rat, human and rabbit Na^+-glucose cotransporters, *Am. J. Physiol. 270*, G919−G926.
23. Díez-Sampedro, A., Lostao, M. P., Wright, E. M., and Hirayama, B. A. (2000) Glycoside binding and translocation in Na^+-dependent glucose cotransporters: comparison of SGLT1 and SGLT3, *J. Membr. Biol. 176*, 111−117.
24. Mackenzie, B., Loo, D. D. F., and Wright, E. M. (1998) Relationships between Na^+/glucose cotransporter (SGLT1) currents and fluxes, *J. Membr. Biol. 162*, 101−106.
25. Gagnon, D. G., Holt, A., Bourgeois, F., Wallendorff, B., Coady, M. J., and Lapointe, J.-Y. (2005) Membrane topology of loop 13−14 of the Na^+/glucose cotransporter (SGLT1): A SCAM and fluorescent labelling study, *Biochim. Biophys. Acta 1712*, 173−184.
26. Puntheeranurak, T., Kasch, M., Xia, X., Hinterdorfer, P., and Kinne, R. K. H. (2007) Three surface subdomains form the vestibule of the Na^+/glucose cotransporter SGLT1, *J. Biol. Chem. 282*, 25222−25230.
27. Schneider, D., and Engelman, D. M. (2004) Motifs of two small residues can assist but are not sufficient to mediate transmembrane helix interactions, *J. Mol. Biol. 343*, 799−804.
28. Eskandari, S., Wright, E. M., and Loo, D. D. F. (2004) Kinetics of the reverse mode of the Na^+/glucose cotransporter, *J. Membr. Biol. 204*, 23−32.
29. Sauer G. A., Nagel G., Koepsell H., Bamberg E., Hartung K. (2000) Voltage and substrate dependence of the inverse transport mode of the rabbit Na^+/glucose cotransporter (SGLT1), *FEBS Lett. 469*, 98−100.
30. Quiocho, F. (1989) Protein-carbohydrate interactions: basic molecular features, *Pure Appl. Chem. 61*, 1293−1306.
31. Taroni, C., Jones, S., and Thornton, J. M. (2000) Analysis and prediction of carbohydrate binding sites, *Protein Eng. 13*, 89−98.
32. Abramson, J., Smirinova, I., Kasho, V., Verner, G., Kaback, H. R., and Iwata, S. (2003) Structure and mechanism of the lactose permease of *Escherichia coli*, *Science 301*, 610−615.
33. Jung, K., Jung, H., Colacurcio, P., and Kaback, H. R. (1995) Role of glycine residues in the structure and function of lactose permease, an *Escherichia coli* membrane transport protein, *Biochemistry 34*, 1030−1039.
34. Voss, A. A., Díez-Sampedro, A., Hirayama, B. A., Loo, D. D. F., and Wright, E. M. (2007) Imino sugars are potent agonists of the human glucose sensor SGLT3, *Mol. Pharmacol. 71*, 628−634.
35. Lostao, M. P., Hirayama, B. A., Loo, D. D. F., and Wright, E. M. (1994) Phenylglucosides and the Na^+/glucose cotransporter (SGLT1): analysis of interactions, *J. Membr. Biol. 142*, 161−170.
36. Yernool, D., Boudkar, O., Jin, Y., and Gouaux, E. (2004) Structure of a glutamate transporter homologue from *Pyrococcus horikoshii*, *Nature 431*, 811−818.
37. Yamashita, A., Singh, S. K., Kawate, T., and Gouaux, E. (2005) Crystal structure of a bacterial homologue of Na^+/Cl^--dependent neurotransmitter transporters, *Nature 437*, 215−223.

BI701562K